Virologica Sinica 37 (2022) 804–812

Contents lists available at ScienceDirect

Virologica Sinica

journal homepage: www.keaipublishing.com/en/journals/virologica-sinica
www.virosin.org

Research Article

Characteristics of replication and pathogenicity of SARS-CoV-2 Alpha and Delta isolates

Xiao-Li Feng [a,1], Dandan Yu [a,b,f,1], Mi Zhang [c,1], Xiaohong Li [b,1], Qing-Cui Zou [a], Wentai Ma [d,i], Jian-Bao Han [a], Ling Xu [a,b,f], Cuixian Yang [c], Wang Qu [a], Zhong-Hua Deng [a], Junyi Long [a], Yanghaopeng Long [a], Mingkun Li [d,e], Yong-Gang Yao [a,b,f,g], Xing-Qi Dong [c,*], Jianxiong Zeng [a,b,f,g,h,*], Ming-Hua Li [a,*]

[a] Kunming National High-level Biosafety Research Center for Non-Human Primates, Center for Biosafety Mega-Science, Kunming Institute of Zoology, Chinese Academy of Sciences, Kunming, 650107, China
[b] Key Laboratory of Animal Models and Human Disease Mechanisms of the Chinese Academy of Sciences, and KIZ-CUHK Joint Laboratory of Bioresources and Molecular Research in Common Diseases, Kunming Institute of Zoology, Chinese Academy of Sciences, Kunming, 650201, China
[c] Department of Infectious Diseases, Yunnan Provincial Infectious Diseases Hospital, Kunming, 650301, China
[d] Key Laboratory of Genomic and Precision Medicine, Beijing Institute of Genomics, Chinese Academy of Sciences, and China National Center for Bioinformation, Beijing, 100101, China
[e] Center for Excellence in Animal Evolution and Genetics, Chinese Academy of Sciences, Kunming, 650201, China
[f] National Resource Center for Non-Human Primates, National Research Facility for Phenotypic & Genetic Analysis of Model Animals (Primate Facility), Kunming Institute of Zoology, Chinese Academy of Sciences, Kunming, 650107, China
[g] Kunming College of Life Science, University of Chinese Academy of Sciences, Kunming, 650204, China
[h] Yunnan Key Laboratory of Biodiversity Information, Kunming Institute of Zoology, Chinese Academy of Sciences, Kunming, 650201, China
[i] University of Chinese Academy of Sciences, Beijing, 100049, China

ARTICLE INFO

Keywords:
SARS-CoV-2
Variants of concern (VOC)
Alpha
Delta
hACE2 transgenic mice
Hamster

ABSTRACT

The continuously arising of SARS-CoV-2 variants has been posting a great threat to public health safety globally, from B.1.17 (Alpha), B.1.351 (Beta), P.1 (Gamma), B.1.617.2 (Delta) to B.1.1.529 (Omicron). The emerging or re-emerging of the SARS-CoV-2 variants of concern is calling for the constant monitoring of their epidemics, pathogenicity and immune escape. In this study, we aimed to characterize replication and pathogenicity of the Alpha and Delta variant strains isolated from patients infected in Laos. The amino acid mutations within the spike fragment of the isolates were determined via sequencing. The more efficient replication of the Alpha and Delta isolates was documented than the prototyped SARS-CoV-2 in Calu-3 and Caco-2 cells, while such features were not observed in Huh-7, Vero E6 and HPA-3 cells. We utilized both animal models of human ACE2 (hACE2) transgenic mice and hamsters to evaluate the pathogenesis of the isolates. The Alpha and Delta can replicate well in multiple organs and cause moderate to severe lung pathology in these animals. In conclusion, the spike protein of the isolated Alpha and Delta variant strains was characterized, and the replication and pathogenicity of the strains in the cells and animal models were also evaluated.

1. Introduction

The COVID-19 pandemic is being persistent by the emerging variants of concern (VOC). The SARS-CoV-2 mutant strains have elevated disease-causing capacity compared to the prototype, for example higher transmissibility, faster replication and reduced neutralization (Tao et al., 2021; Harvey et al., 2021). These mutations mainly occurred in the spike protein that mediates viral attachment and entry into host cells via the ACE2 receptor. The D614G mutation of the spike protein remarkably increased binding to the host hACE2 receptor early in the pandemic (Zhang et al., 2020) and was quick to become a dominant variant circulating around the world. Several potential variant strains like B.1.621 (Mu) (Xie et al., 2021) were monitored and, however, did not cause severe pandemic globally. Subsequently, B.1.1.7 (Alpha)

* Corresponding authors.
E-mail addresses: dongxq8001@126.com (X.-Q. Dong), zengjianxiong@mail.kiz.ac.cn (J. Zeng), limh@mail.kiz.ac.cn (M.-H. Li).
[1] Xiao-Li Feng, Dandan Yu, Mi Zhang and Xiaohong Li contributed equally to this work.

https://doi.org/10.1016/j.virs.2022.09.007
Received 13 June 2022; Accepted 20 September 2022
Available online 24 September 2022

variant was initially identified in the United Kingdom in September 2020 and fast got transmitted globally in early 2021 (Kraemer et al., 2021; van Loon et al., 2021). Another two VOCs called B.1.351 (Beta) and P.1 (Gamma) were first identified in South Africa and Japan/Brazil, respectively (da Silva et al., 2021; Tegally et al., 2021), and were greatly concerned initially because both demonstrated unprecedented ability to diminish efficacy of COVID-19 vaccines at that time (Charmet et al., 2021; Hall et al., 2021; Hitchings et al., 2021; Madhi et al., 2021; Sadoff et al., 2021; Shinde et al., 2021). Alpha and Beta strains harbor the N501Y mutations in their spike protein and have also been reported to result in more severe symptoms in humans (Grint et al., 2021; Patone et al., 2021) and animal models (Liu et al., 2022b; Bayarri-Olmos et al., 2021; Radvak et al., 2021) including human ACE2 (hACE2) transgenic mice and hamsters.

When Alpha, Beta and Gamma strains were continuously circulating globally, B.1.617.2 (Delta) was initially identified in India (Singh et al., 2021) and caused a sharp rise of COVID-19 cases from India to the rest of the world. It was frustrating at that time that Delta was capable of resulting in breakthrough infection for those who, despite, were fully vaccinated before, largely by compromising the protective efficacy of several prevalent COVID-19 vaccines such as ChAdOx1, mRNA-1273 and BNT162b2 (Bernal et al., 2021; Dagan et al., 2021; Sheikh et al., 2021; Tang et al., 2021). Thus, different from previous circulating variants, Delta posted a great threat to both unvaccinated and vaccinated populations, further adding the uncertainty in global fight against COVID-19. The occurrence of highly transmission and pathogenicity of Delta relied on the critical mutations in its spike protein, which were partially shared with other VOC (Deng et al., 2021; Greaney et al., 2021). These key mutations markedly endowed Delta strain with increased transmissibility and reduced antibody neutralization (Planas et al., 2021). In addition to the D614G substitution, P681R mutation in Delta spike protein was proven to promote binding affinity to ACE2 receptor and cellular entry (Saito et al., 2022). A new SARS-CoV-2 variant B.1.1.529 (Omicron) was documented on November 24 in 2021 from Botswana and South Africa and classified as the fifth VOC just two days later. Omicron strain possesses an unprecedented 30 amino acid substitutions in its spike protein compared with the prototype and 15 of these mutations occurred in the receptor-binding domain (RBD) (Lin et al., 2022; Zhao et al., 2022), suggesting the possibility of biological changes of Omicron. Unsurprisingly, Omicron has been reported to robustly escape from multiple vaccines and therapeutic neutralization antibodies (Andrews et al., 2022; Wang et al., 2022; Muik et al., 2022) although with attenuated replication and pathogenicity in animal models.

The emergence or re-emergence of the VOC strains internally requires the persistent monitoring of SARS-CoV-2 variants in clinic. In this study, we isolated two SARS-CoV-2 variant strains from patients infected in Laos and identified the Alpha and Delta variants by decoding the mutations of the spike protein. Both variant isolates can replicate efficiently in multiple cells and organs and cause moderate to severe lung pathology in hACE2 transgenic mice and hamsters.

2. Materials and methods

2.1. Cell culture

Huh-7, HPA-3, Caco-2, and Vero E6 cells were introduced from Kunming Cell Bank and Calu-3 was purchased from Procell Life Science & Technology Co., Ltd. Cells were grown in Dulbecco's Modified Eagle medium (DMEM) high glucose (Gibco, Beijing) supplemented with 10% fetal bovine serum (FBS) (Gibco, New Zealand), 1% penicillin/streptomycin (Solarbio, Beijing), and kept in a humidified 5% CO_2 incubator at 37 °C.

2.2. Virus isolation and identification

The suspected SARS-CoV-2-containing clinical specimens (nasopharyngeal swabs) were used for virus isolation. The nasopharyngeal swabs were inoculated in Vero E6 cell lines and cultured in DMEM supplemented with 2% FBS and final concentrations of penicillin 100 units/mL, streptomycin 100 μg/mL. The culture was checked for cytopathic effect (CPE) daily. Once the CPE was observed, 200 μL cell culture supernatant was used for total nucleic acid extraction and Sanger sequencing for the confirmation of the presence of SARS-CoV-2. Furthermore, the virus was passaged three more times to obtain a working stock.

As for the whole genome sequencing of the variant isolates, the viral genomic RNA was extracted from viral culture supernatant using a high pure viral RNA kit (Roche, 11858882001, Germany) and purified according to the manufacturer's instructions. After that, the next-generation sequencing (NGS) library was prepared using a MultipSeq® Custom Panel (A186XV7) for BGI Platporm (iGeneTech). The sequencing was performed using a NovaSeq 6000 Sequencing System (Illumina). All sequencing reads were mapped to the SARS-CoV-2 reference genome (MN908947.3) using Mininap2 (v2.1) (Li, 2018), and alleles with a frequency greater than 70% were designated as the consensus. The average sequencing depth on the viral genome was higher than 36,000-fold, and over 99.8% of the genomic region was covered by at least five-folds for the two samples. Mutations were called at positions with a minimum sequencing depth of 5-folds and a minimum frequency of 70% was required. Sequences alignment was done by Mafft (v7.453) (Katoh and Standley, 2013). The phylogenetic reconstruction was performed using 3087 representative global sequences retrieved from Nextstrain (https://nextstrain.org; as of 8th February 2022) and the two consensus genomes obtained in the current study using IQTREE (v1.6.12) (Nguyen et al., 2015).

The infectious titers of the variant isolates were quantified by an endpoint titration assay. Briefly, serial 10-fold dilutions of cultured SARS-CoV-2 stock were prepared using viral culture media and added into seeded 96-well plates. The 96-well plates were cultured at 37 °C (5% CO_2) for 5–6 days and then observed for CPE. The 50% tissue culture infectious dose ($TCID_{50}$) was finally calculated by the Reed-Muench method (Reed and Muench, 1938).

The prototyped SARS-CoV-2 strain was kindly provided by Guangdong Provincial Center for Disease Control and Prevention, Guangdong Province of China and was described in our previous studies (Xu et al., 2020; Song et al., 2020). The virus was propagated and titrated in Vero E6 cells, which were cultured in DMEM supplemented with 2% FBS. The viral sequence is accessible in the China National Microbiology Data Center (Accession No. NMDCN0000HUI).

2.3. Viral growth curves

The replication kinetics of the two isolated SARS-CoV-2 variants were evaluated in a growth curve and compared with the prototyped strain. In brief, Vero E6, Calu-3, Caco-2, Huh-7, HPA-3 and Vero E6 cells were infected with the two variant isolates and prototyped strain at a multiplicity of infection 0.1 (MOI 0.1), respectively, and the viral replication was evaluated every 12 h for 72 h post-inoculation using a quantitative real-time PCR (qRT-PCR) method.

2.4. Animal models

Twenty-four male hACE2 transgenic mice [C57BL/6-Tgtn(CAG-human ACE2-IRES-Luciferase-WPRE-polyA)Smoc] (8–12 weeks old) from the Shanghai Model Organisms and 24 golden hamsters (6–8 weeks old, male) from Beijing Vital River Laboratory Animal Technology Co., Ltd were maintained in the Experimental Animal Core Facility of the Kunming Institute of Zoology (KIZ), Chinese Academy of Sciences (CAS). The hACE2 mouse model used in our experiments was driven by CAG promoter and established via random transgenic technologies, which had a stable expression of hACE2 in multiple organs. For SARS-CoV-2 infections, all these animals were maintained at the ABSL-3 animal core facility of the KIZ on a 12-h light/dark cycle, with free access to food and water. After anesthetization with isoflurane (RWD Life Science,

Shenzhen), each group of mice or hamsters (n = 6) were intranasally infected with a total of 20 μL viral stock containing 1×10^4 $TCID_{50}$ of SARS-CoV-2 prototype or variants. Body temperature and weight of all mice were recorded daily until sacrifice at three days post infection. Blood samples were collected for routine blood tests before infection and just before sacrifice. Tissue samples were collected from animals after euthanasia and stored in −80 °C freezer (for quantification of mRNA and protein levels) or in 4% paraformaldehyde (PFA; for histological analysis and immunofluorescence) until use, as described in our previous studies (Xu et al., 2020; Xie et al., 2021).

2.5. Quantitative real-time PCR (qRT-PCR)

Total RNA was extracted from homogenized mouse tissues using a TRIzol reagent (ThermoFisher Scientific, America). SARS-CoV-2 RNAs were detected by one-step RT-PCR using a THUNDERBIRD Probe One-Step qRT-PCR (TOYOBO, Japan) following the manufacturer's protocols. The total viral genomic RNA (gRNA) gene primers targeting the N protein described in our previous studies (Xu et al., 2020; Zeng et al., 2022) were used, including 5′-GGGGAACTTCTCCTGCTAGAAT-3′, 5′-CAGACATTTTGCTCTCAAGCTG-3′, probe 5′-FAM-TTGCTGCTGCTTGACAGATT-TRMRA-3′. The viral sub-genomic RNA (sgRNA) gene primers targeting the E protein were used, including 5′- CGATCTCTTGTAGATCTGTTCTC-3′, 5′-ATATTGCAGCAGTACGCACACA-3′, probe 5′- FAM-ACACTAGCCATCCTTACTGCGCTTCG-TAMRA-3′. Serial dilutions of the SARS-CoV-2 RNA reference standard (National Institute of Metrology, China) were used in each run, in parallel to calculate copy numbers in each sample on ViiA 7 Real-Time PCR System (Applied Biosystems).

2.6. Histological analysis

We followed the same histological approach as described in our previous studies (Song et al., 2020; Xu et al., 2020). In brief, lung and brain tissues form SARS-CoV-2-infected mice or hamsters were fixed in 4% PFA (Biosharp) for at least 7 days, and then were paraffin embedded (ThermoFisher Scientific) and cut into 3-μm sections following the standard procedure (RWD Life Science). The tissue slides were stained with H&E (Solarbio, Beijing) and imaged by the Leica DM 6B light microscopy.

2.7. Immunofluorescence

Immunofluorescence was performed as described in our previous studies (Zeng et al., 2019, 2020; Xu et al., 2020). Briefly, the sections were deparaffinized in xylene and rehydrated through a graded ethanol series. For antigen retrieval, sections immersed in saline sodium citrate buffer were microwave heated for 10 min three times. After cooled to room temperature, the sections were washed by 1 × phosphate-buffered saline (PBS) and blocked with 5% bovine serum albumin (BSA) in 1 × PBST (0.3% Triton-X 100 in PBS) at 37 °C for 60 min. The commercial anti-nucleocapsid antibody (1:500, Catalog # A20021, ABclonal, Wuhan) were diluted in 3% BSA in 1 × PBST (0.2% Triton-X 100) and incubated overnight at 4 °C. The sections were then washed, and immunoreactivity was detected using Donkey anti-Rabbit IgG Highly Cross-Adsorbed Secondary Antibody, Alexa Fluor Plus 555 (1:500; Thermo Fisher Scientific) for 1 h at room temperature. The sections were counterstained with 5 μg/mL 4′,6-diamidino-2-phenylindole (DAPI; Thermo Fisher Scientific) for 10 min at room temperature and washed with 1 × PBST (0.2% Triton-X 100) three times. Slides were visualized using ZEISS LSM880 confocal microscope.

2.8. Statistical analysis

All appropriate data were analyzed using GraphPad Prism 8 (GraphPad Software Inc.). All hypothesis tests were performed as two-tailed tests. Specific statistical analysis methods are described in the figure legends where results are presented. Values were considered statistically significant for P values < 0.05.

3. Results

3.1. Identification of the spike mutations of the SARS-CoV-2 Alpha and Delta isolates

To monitor the epidemic features of SARS-CoV-2 variants, we tentatively isolated the variants in suspected SARS-CoV-2-containing nasopharyngeal swabs from patients infected in Laos. With the observation of the CPE in Vero E6 cells inoculated with two samples, total cellular RNA of each sample was purified and subjected to deep sequencing. The sequencing data (3087 genomes) were assembled and aligned with viral genomes of the existed SARS-CoV-2 variants by Nextstrain (https://nextstrain.org/) on Feb 8, 2022. As a result, two isolates were identified to belong to Alpha and Delta variants, respectively (Fig. 1A). Phylogenetic tree analysis within Nextstrain database (https://nextstrain.org/) showed that the Alpha (DWS1216) and Delta (DWSJ070) isolates were most close to one isolated from Cambodia (KHM B117 2021) (Supplementary Fig. S1) and from Georgia (USA GA GPHL 2509 2021) and Utah (USA UT CDC ASC210489950 2021) (Supplementary Fig. S2), respectively. Furthermore, nucleotide alignment analysis revealed that spike (S) protein of the Alpha isolate included three amino acid deletions at 69 and 70 (Δ69–70) and 144 (Δ144) sites, and five amino acid substitutions (G261C, N501Y, A570D, D614G and P681H) in the S1 subunit, and three amino acid substitutions (T716I, S982A and D1118H) in the S2 subunit (Fig. 1B). Two amino acid deletions at 157 and 158 (Δ157–158), five amino acid deletions from 675 to 679 (Δ675–679) sites, and nine amino acid substitutions (T19R, T95I, G142D, W258L, K417N, L452R, T478K, D614G and P681R) in the S1 subunit, and two amino acid substitutions (D950N and T1117I) in the S2 subunit were identified in the S protein of the Delta isolate (Fig. 1B). Taken together, we isolated two SARS-CoV-2 variants from the nasopharyngeal samples and identified them as Alpha and Delta variants, respectively.

3.2. The Alpha and Delta isolates are replicated differentially in multiple cells

To evaluate the replication capacity of the SARS-CoV-2 isolates, we performed a viral growth curve by examining viral titers in multiple cells that have been most used in SARS-CoV-2 infection at an MOI of 0.1 (Sasaki et al., 2021; Shuai et al., 2022). In lung Calu-3 cells, the Alpha and Delta isolates replicated faster than the prototyped SARS-CoV-2 that was described in our previous studies (Zeng et al., 2022; Xu et al., 2020) within initial 12 h post-infection (hpi), and thereafter replication of the Alpha and Delta isolates slowed down compared to the prototype (Fig. 2A). Similar replication features of the Alpha and Delta isolates were also observed in Caco-2 cells (Fig. 2B). In Huh-7 cells, the prototype showed a higher replication capacity than the Alpha and Delta isolates from 12 to 72 hpi (Fig. 2C). The Delta isolate replicated faster especially from 36 to 60 hpi than the prototype and Alpha isolate that were indistinguishable regarding replication capacity in Vero E6 cells (Fig. 2D). However, we did not observe the replication of the prototype and the Alpha and Delta isolates since 12 hpi in HPA-3 cells (Fig. 2E). Taken together, the Alpha and Delta isolates replicated differentially in the multiple cells.

3.3. Viral replication of Alpha and Delta isolates in multiple organs of hACE2 transgenic mice and hamsters

To examine replication of the Alpha and Delta isolates *in vivo*, we intranasally infected hACE2 transgenic mice and hamsters with a titer of 1×10^4 $TCID_{50}$ for each isolate. Animals were euthanized three days after infection. We observed that body weight of the hACE2 transgenic mice infected with the prototype and Delta isolates decreased compared to the

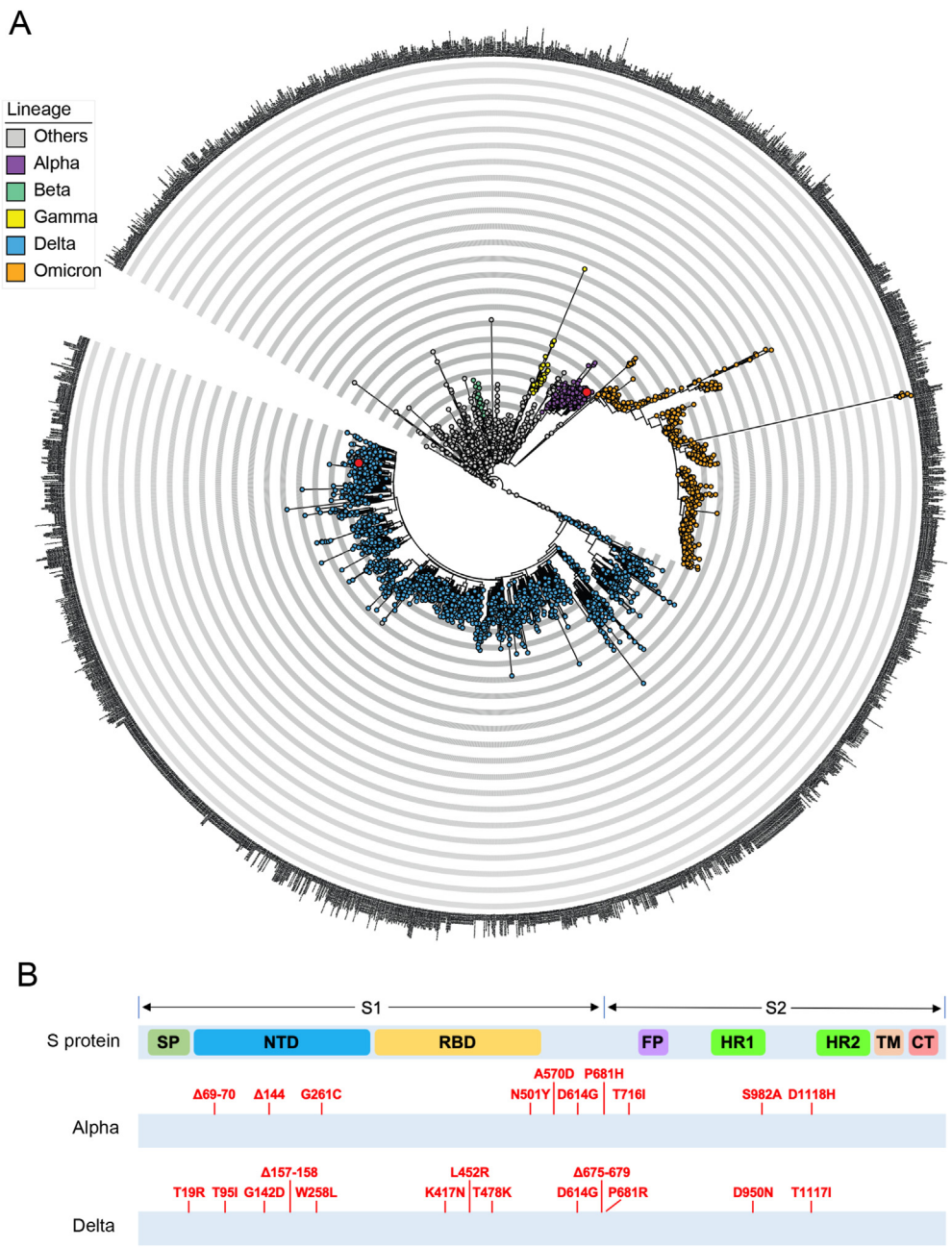

Fig. 1. Identification of the spike (S) mutations in the SARS-CoV-2 isolates. **A** Phylogenetic analysis of the spike sequences of the SARS-CoV-2 isolates within the existed SARS-CoV-2 variants by Nextstrain (https://nextstrain.org/). Red circles indicate the SARS-CoV-2 isolates in this study. **B** Schematic diagram showing the spike mutations in the Alpha and Delta isolates compared to the prototyped SARS-CoV-2. SP, signal peptide; NTD, N-terminal domain; RBD, receptor-binding domains; FP, fusion peptide; HR1, heptapeptide repeat sequence 1; HR2, heptapeptide repeat sequence 2; TM, transmembrane domain; CT, cytoplasmic domain.

uninfected mice at 3 dpi, while body weight of the Alpha isolate-infected mice kept unchanged (Supplementary Fig. S3A). Nevertheless, body weight of hamsters that were infected with the prototype and the Alpha and Delta isolates was indistinguishable compared to the uninfected ones at 3 dpi (Supplementary Fig. S3B). We next quantified the SARS-CoV-2 genomic RNA (gRNA) or sub-genomic RNA (sgRNA) within multiple organs of hACE2 transgenic mice and hamsters. The Alpha and Delta isolates showed an identical replication capacity with a comparable gRNA and sgRNA to the prototype in the lungs of the mice and hamsters (Fig. 3A and B). However, we observed a differentiated replication dynamics in the brains of the mice and hamsters, whereas the Alpha and Delta isolates showed decreased and increased viral load, respectively, compared to the prototype in the mice. The Delta isolate, but not the Alpha, showed reduced replication compared to the prototype in the hamsters (Fig. 3C). In heart, we observed a similar replication feature that the Delta isolate replicated lower than either the prototype or the Alpha in the mice and hamsters (Fig. 3D). Additionally, we did not observe the difference of the replication between the Alpha and Delta isolates and the prototype in the kidney and duodenum of the mice. The Delta isolate had a decrease of viral load compared to the prototype in the hamsters, while such decrease was also observed for the Alpha isolate only in the duodenum but not in kidney (Fig. 3E and F). However, viral load of the Alpha and Delta isolates was similar to the prototype in both liver and spleen of the mice and hamsters (Fig. 3G and H).

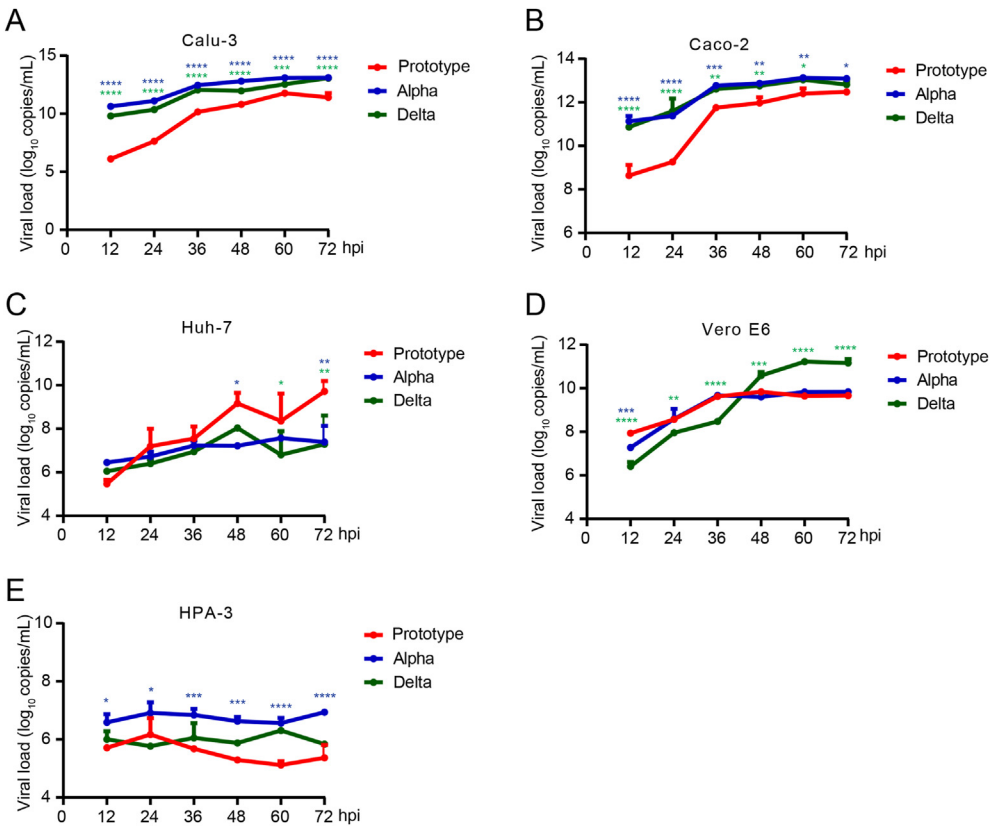

Fig. 2. Viral growth curves of the SARS-CoV-2 isolates in multiple cells. **A–E** The Calu-3 (**A**), Caco-2 (**B**), Huh-7 (**C**), Vero E6 (**D**) and HPA-3 (**E**) cells were infected with the prototype SARS-CoV-2, the Alpha or Delta isolate at an MOI of 0.1. Total cellular RNAs were collected at the indicated timepoints to quantify the SARS-CoV-2 genome. Data were shown as mean ± standard deviation (n = 2). Statistical analysis was performed by two-way ANOVA with Bonferroni's *post hoc* test. *$P < 0.05$, **$P < 0.01$, ***$P < 0.001$, ****$P < 0.0001$. The *P* values marked in green color refer to the comparisons between the prototype SARS-CoV-2 and the Delta isolate, and the values marked in blue refer to the comparisons between the prototype SARS-CoV-2 and the Alpha isolate.

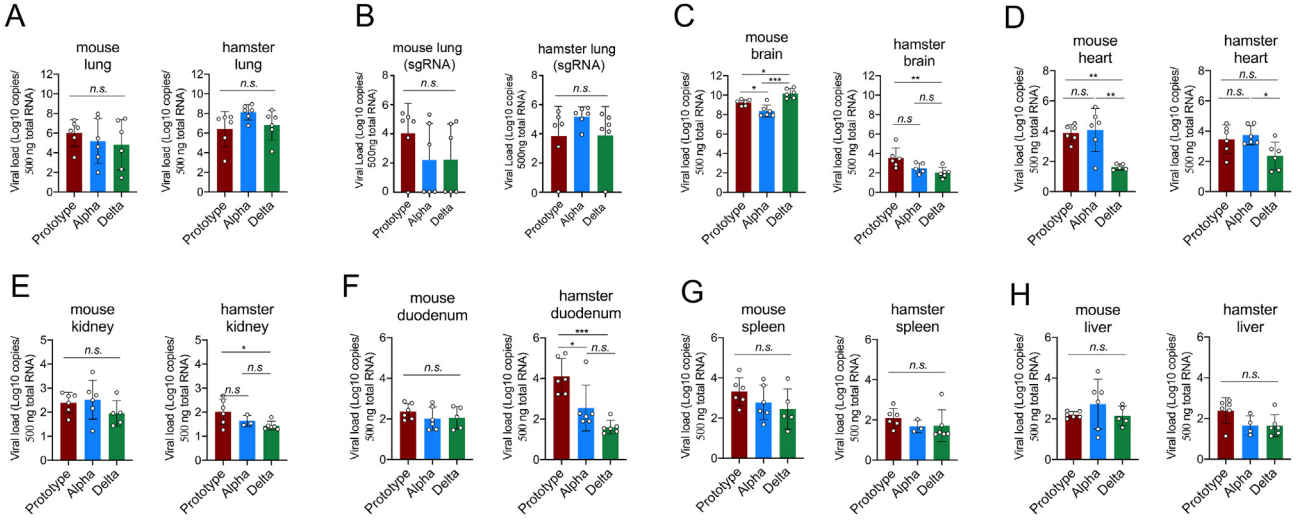

Fig. 3. Viral loads of Alpha and Delta isolates in multiple organs of hACE2 transgenic mice and hamsters. **A–H** Viral load (gRNA) of the Alpha and Delta isolates in lung (**A**), brain (**C**), heart (**D**), kidney (**E**), duodenum (**F**), spleen (**G**) and liver (**H**) tissues in infected hACE2 transgenic mice (left panel) and hamsters (right panel) at 3 dpi, as determined by quantitative real time-PCR. **B** Quantification of SARS-CoV-2 subgenomic RNA (sgRNA) in lung tissues of the prototype SARS-CoV-2-, Alpha- and Delta-infected hACE2 transgenic mice (left panel) and hamsters (right panel). Values are presented as mean ± standard deviation; n = 6 (with exclusion of some samples in certain group having missing data, so that the dots in each bar showed inconsistent numbers). Statistical analysis was performed by one-way ANOVA with Bonferroni's *post hoc* test. n.s., not significant, *$P < 0.05$, **$P < 0.01$, ***$P < 0.001$.

3.4. Pathology of the Alpha and Delta isolates in hACE2 transgenic mice and hamsters

We first determined SARS-CoV-2 replication by examining the viral nucleocapsid protein via immunofluorescence assay. The results showed that, similar to the prototype, expression of the nucleocapsid protein of the Alpha and Delta isolates was abundantly present in lung cells (Fig. 4), demonstrating that the Alpha and Delta isolates can replicate efficiently in lungs. To further examine pathogenicity of the Alpha and Delta isolates *in vivo*, we performed hematoxylin and eosin (H&E) staining for histopathology in lung sections of the infected mice and hamsters. Compared to the uninfected mice, severe interstitial pneumonia with thickened alveolar septa, severe infiltration of inflammatory immune cells, and moderate interstitial congestion were observed in lungs of the prototype-infected mice, while the Alpha isolate-infected lungs showed relative moderate interstitial pneumonia but severe interstitial congestion. Infection of the Delta isolate caused severe interstitial pneumonia with thickened alveolar septa and infiltration of inflammatory immune cells, and obviously more severe interstitial congestion than the prototype and Alpha isolate in the lungs of the mice (Fig. 5A). In hamsters, severe interstitial pneumonia with thickened alveolar septa, severe infiltration of inflammatory immune cells, and severe interstitial congestion were observed in the prototype-, the Alpha-, and the Delta-infected lungs, and the severity was overall indistinguishable between them (Fig. 5B). These results demonstrated that the Alpha and Delta isolates could infect lung tissues and cause detectable lung pathology in hACE2 transgenic mice and hamsters.

We also evaluated whether the infection of the prototype, the Alpha, and the Delta isolates would cause potential brain pathologies in addition to lung pathology in the hACE2 transgenic mice and hamsters. The H&E staining for the brain sections of the infected animals did not show very severe brain pathologies. Yet we observed a few pathological features related to neuronal degeneration in some brain sections (Fig. 5C). Furthermore, we found the occurrence of neuroinflammation as indicated by gliosis in some brain sections of prototype- and Alpha-infected mice, but not in the Delta-infected mice (Fig. 5D). These preliminarily pathological results suggest that long-term outcome of SARS-CoV-2 infection on brain deserves to be further evaluated.

4. Discussion

With the persistent mutations of the spike protein responsible for cell entry and immune escape under the evolutionary pressure from host (Shu et al., 2021; Castiglione et al., 2021), it is important to monitor SARS-CoV-2 variants globally (Tao et al., 2021). In the present study, the Alpha and Delta variants that were isolated from nasopharyngeal samples in Laos were characterized by replication kinetics in multiple cells and pathogenicity in both hACE2 transgenic mice and hamsters. Our live virus infection assays revealed that the replication of the Alpha and Delta isolates was dramatically increased in Calu-3 and Caco-2 cells. This result is in agreement with the previous reports and preprints that demonstrated an enhanced infectivity of Alpha- and Delta-pseudovirus or live Alpha and Delta variants in Calu-3 and Caco-2 cells (de Souza et al., 2022; Lubinski et al., 2022; Rajah et al., 2021). However, such impact was not similarly observed for the Alpha and Delta isolates in Huh-7, Vero E6 and HPA-3 cells. These results suggested that the SARS-CoV-2 variants possessed different replication kinetics between cells.

The Alpha and Delta isolates that we identified in the present study showed several different mutation features of the spike protein from the corresponding reference variants from the WHO. Compared to the referenced Alpha variant, where the deletion or mutations of the spike protein includes Δ69–70, Δ144, N501Y, A570D, D614G, P681H, T716I, S982A and D1118H, the newly mutation of G261C was present in the Alpha isolate. In addition, the Delta isolate had the newly mutations of T95I, G142D, W258L, K417N and T1117I in the spike protein compared to the referenced Delta variant (Planas et al., 2021). Although it is now in details unknown whether these newly mutations have an effect on viral biological features such as the binding affinity to ACE2 receptor and the resistance to neutralizing antibody, the Alpha and Delta isolates showed similar replication kinetics in Calu-3 and Caco-2 cells and pathogenicity in animal models as described in the present study when compared to the previous studies on their referenced counterparts (de Souza et al., 2022; Lubinski et al., 2022; Rajah et al., 2021). These results suggested that both SARS-CoV-2 variant isolates would be appropriate to be used in the evaluation of anti-viral drugs or vaccines in cells and animals.

Studies have shown that K417N mutation is present in spike of a sub-lineage of Delta variant, called Delta plus (Delta+) (Moyo-Gwete et al., 2022). Further, this mutation also exists within spike of Beta (B.1.351) (Liu et al., 2022a) and all Omicron variants including BA.1, BA.2, BA.4, BA.5, and BA.2.12.1 (Kumar et al., 2022) (Supplementary Fig. S4). Previous studies have shown K417N mutation led to reduced cellular immune responses (Zhang et al., 2021) while might moderately decrease the binding affinity to human ACE2 (Han et al., 2022). Another preprint reported that several Omicron spike mutations including K417N were very disruptive to therapeutic monoclonal antibodies (Chen and Wei, 2022). These existing clues suggest that K417N mutation could confer the Delta isolate in our current study with known biological function, which should be noted when it will be used to evaluate COVID-19 vaccines.

SARS-CoV-2 Alpha and Delta variants that we isolated can effectively replicate in the cell lines and multiple organs of infected animal models

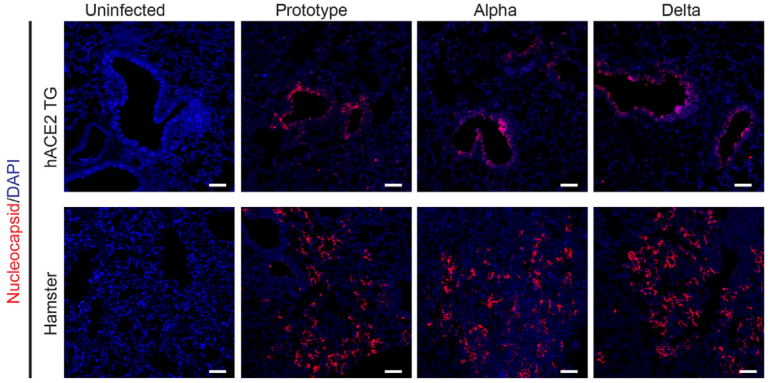

Fig. 4. Viral protein of the SARS-CoV-2 isolates in infected hACE2 transgenic mice and hamsters. Immunofluorescence assay examined the SARS-CoV-2 nucleocapsid protein of lung tissues in the prototype-, Alpha- and Delta-infected hACE2 transgenic mice (upper panel) and hamsters (bottom panel) at 3 dpi. The uninfected lung tissues were used as control. Scale bar, 100 μm. Nuclei were stained by DAPI.

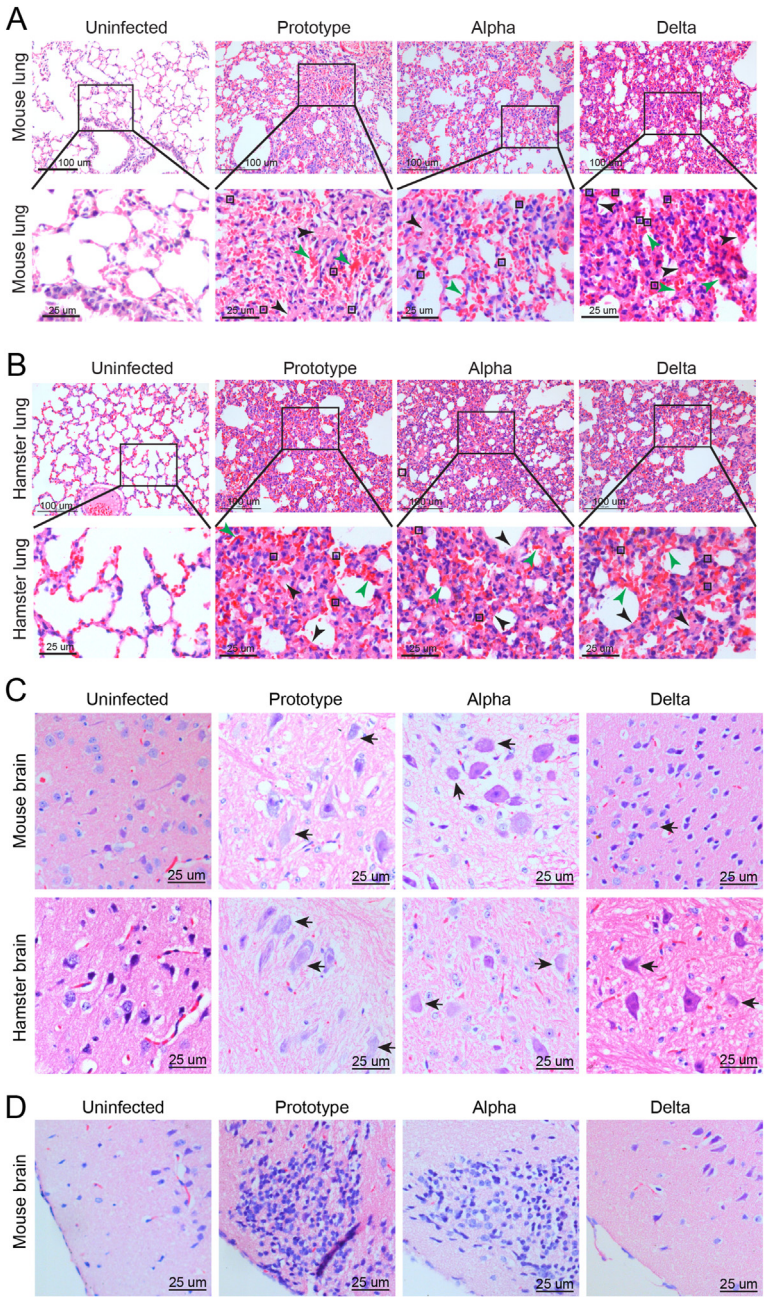

Fig. 5. Histopathology of lung and brain tissues in the Alpha- and Delta-infected hACE2 transgenic mice and hamsters. **A, B** Histopathology of lung tissues from the prototype SARS-CoV-2, the Alpha isolate, or the Delta isolate infected hACE2 transgenic mice (**A**) and hamsters (**B**) at 3 dpi. The uninfected lung tissues were used as control. Histopathological observations indicated the presence of interstitial pneumonia with thickened alveolar septa (black arrow), interstitial congestion (green arrow), and infiltration of lymphocytes (black frames). Scale bar, 25 or 100 μm as indicated. **C, D** H&E staining for brains of hACE2 transgenic mice and hamsters infected with the indicated viruses showed neuronal degeneration as indicated by black arrows (**C**) and gliosis (**D**). Scale bar, 25 μm.

and consequently cause detectable lung pathology. For *in vitro* infection assay, we found that the Alpha and Delta variants replicated more effectively than the prototype in Calu-3 and Caco-2 cells, likely due to higher affinity between their spike and human ACE2 (Saito et al., 2022). This observation is consistent with the results from the recent study (Shuai et al., 2022) where several SARS-CoV-2 variants including Alpha and Delta were evaluated in the same cells. Furthermore, we performed *in vivo* assay and found no significant difference regarding sgRNA copies and pathology of lung tissues between Alpha and Delta and the prototype in hACE2 transgenic mice and hamsters. Such phenotypes were similarly observed in K18-hACE2 transgenic mice (Shuai et al., 2022) in which a comparable viral sgRNA copies were documented between Delta and the wild-type virus in nasal turbinate and lung.

5. Conclusions

In conclusion, we isolated the Alpha and Delta variants from Laos and their key features of the spike protein sequences have been decoded. Both variant isolates can replicate efficiently in multiples cells and cause moderate to severe lung pathology in the models of mice and hamsters.

Data availability

The sequencing data of the Alpha and Delta isolates were deposited in the National Microbial Data Center (NMDC) with accession number NMDC60042792 and NMDC60042793.

Ethics statement

All experiments with live SARS-CoV-2 were conducted in the animal biosafety level 3 (ABSL3) facility in the KIZ, CAS. The Institutional Animal Care and Use Committee of KIZ, CAS, approved all experimental procedures and protocols used in this study (Approval No. IACUC-RE-2021-12-007).

Author contributions

Xiao-Li Feng: formal analysis, methodology, investigation, visualization, writing-review &editing. Dandan Yu: investigation, visualization. Mi Zhang: resources. Xiaohong Li: investigation. Qing-Cui Zou: formal analysis, methodology, investigation, visualization. Wentai Ma: formal analysis, visualization. Jian-Bao Han: investigation. Ling Xu: investigation, visualization. Cuixian Yang: resources. Wang Qu: supervision. Zhong-Hua Deng: supervision. Junyi Long: investigation, supervision. Yanghaopeng Long: investigation, supervision. Mingkun Li: resources. Yong-Gang Yao: conceptualization, funding acquisition, writing-review &editing. Xing-Qi Dong: resources. Jianxiong Zeng: investigation, visualization, writing-original draft. Ming-Hua Li: conceptualization, investigation, validation, project administration.

Conflict of interest

The authors declare no competing interests.

Acknowledgements

We thank Dr. Chang-Wen Ke from Guangdong Provincial Center for Disease Control and Prevention for providing the prototyped SARS-CoV-2 strain. This work was supported by the Major Science and Technique Programs in Yunnan Province (grant No. 202102AA310055), the Bureau of Frontier Sciences and Education, CAS (grant no. QYZDJ-SSW-SMC005 to Y.G.Y.), the Key project of the CAS “Light of West China” Program (to D.Y.) and Yunnan Province (202001AS070023 to D.Y.), and Yunnan Fundamental Research Projects (grant No. 202201AW070020 to J.Z.).

Appendix A. Supplementary data

Supplementary data to this article can be found online at https://doi.org/10.1016/j.virs.2022.09.007.

References

Andrews, N., Stowe, J., Kirsebom, F., Toffa, S., Rickeard, T., Gallagher, E., Gower, C., Kall, M., Groves, N., O'connell, A.M., Simons, D., Blomquist, P.B., Zaidi, A., Nash, S., Aziz, N.I.B.A., Thelwall, S., Dabrera, G., Myers, R., Amirthalingam, G., Gharbia, S., Barrett, J.C., Elson, R., Ladhani, S.N., Ferguson, N., Zambon, M., Campbell, C.N.J., Brown, K., Hopkins, S., Chand, M., Ramsay, M., Bernal, J.L., 2022. Covid-19 vaccine effectiveness against the Omicron (B.1.1.529) variant. N. Engl. J. Med. 2, NEJMoa2119451.

Bayarri-Olmos, R., Johnsen, L.B., Idorn, M., Reinert, L.S., Rosbjerg, A., Vang, S., Hansen, C.B., Helgstrand, C., Bjelke, J.R., Bak-Thomsen, T., Paludan, S.R., Garred, P., Skjoedt, M.O., 2021. The alpha/B.1.1.7 SARS-CoV-2 variant exhibits significantly higher affinity for ACE-2 and requires lower inoculation doses to cause disease in K18-hACE2 mice. Elife 10, e70002.

Bernal, J.L., Gower, C., Andrews, N., 2021. Effectiveness of covid-19 vaccines against the B.1.617.2 (delta) variant. N. Engl. J. Med. 385, e92.

Castiglione, G.M., Zhou, L.L., Xu, Z.H., Neiman, Z., Hung, C.F., Duh, E.J., 2021. Evolutionary pathways to SARS-CoV-2 resistance are opened and closed by epistasis acting on ACE2. PLoS Biol. 19, e3001510.

Charmet, T., Schaeffer, L., Grant, R., Galmiche, S., Cheny, O., Von Platen, C., Maurizot, A., Rogoff, A., Omar, F., David, C., Septfons, A., Cauchemez, S., Gaymard, A., Lina, B., Lefrancois, L.H., Enouf, V., van der Werf, S., Mailles, A., Levy-Bruhl, D., Carrat, F., Fontanet, A., 2021. Impact of original, B.1.1.7, and B.1.351/P.1 SARS-CoV-2 lineages on vaccine effectiveness of two doses of COVID-19 mRNA vaccines: results from a nationwide case-control study in France. Lancet Reg Health Eur 8, 100171.

Chen, J., Wei, G.W., 2022. Omicron BA.2 (B.1.1.529.2): high potential to becoming the next dominating variant. Res Sq 3, rs-1362445.

da Silva, J.C., Felix, V.B., Leao, S., Trindade-Filho, E.M., Scorza, F.A., 2021. New Brazilian variant of the SARS-CoV-2 (P1/Gamma) of COVID-19 in Alagoas state. Braz. J. Infect. Dis. 25, 101588.

Dagan, N., Barda, N., Kepten, E., Miron, O., Perchik, S., Katz, M.A., Hernan, M.A., Lipsitch, M., Reis, B., Balicer, R.D., 2021. BNT162b2 mRNA covid-19 vaccine in a nationwide mass vaccination setting. N. Engl. J. Med. 384, 1412–1423.

de Souza, G.A.P., Le Bideau, M., Boschi, C., Ferreira, L., Wurtz, N., Devaux, C., Colson, P., La Scola, B., 2022. Emerging SARS-CoV-2 genotypes show different replication patterns in human pulmonary and intestinal epithelial cells. Viruses-Basel 14, 23.

Deng, X.D., Garcia-Knight, M.A., Khalid, M.M., Servellita, V., Wang, C.D.C., Morris, M.K., Sotomayor-Gonzalez, A., Glasner, D.R., Reyes, K.R., Gliwa, A.S., Reddy, N.P., San Martin, C.S., Federman, S., Cheng, J., Balcerek, J., Taylor, J., Streithorst, J.A., Miller, S., Sreekumar, B., Chen, P.Y., Schulze-Gahmen, U., Taha, T.Y., Hayashi, J.M., Simoneau, C.R., Kumar, G.R., McMahon, S., Lidsky, P.V., Xiao, Y.H., Hemarajata, P., Green, N.M., Espinosa, A., Kath, C., Haw, M., Bell, J., Hacker, J.K., Hanson, C., Wadford, D.A., Anaya, C., Ferguson, D., Frankino, P.A., Shivram, H., Lareau, L.F., Wyman, S.K., Ott, M., Andino, R., Chiu, C.Y., 2021. Transmission, infectivity, and neutralization of a spike L452R SARS-CoV-2 variant. Cell 184, 3426–3437.

Greaney, A.J., Loes, A.N., Crawford, K.H.D., Starr, T.N., Malone, K.D., Chu, H.Y., Bloom, J.D., 2021. Comprehensive mapping of mutations in the SARS-CoV-2 receptor-binding domain that affect recognition by polyclonal human plasma antibodies. Cell Host Microbe 29, 463–476.

Grint, D.J., Wing, K., Houlihan, C., Gibbs, H.P., Evans, S.J.W., Williamson, E., McDonald, H.I., Bhaskaran, K., Evans, D., Walker, A.J., Hickman, G., Nightingale, E., Schultze, A., Rentsch, C.T., Bates, C., Cockburn, J., Curtis, H.J., Morton, C.E., Bacon, S., Davy, S., Wong, A.Y.S., Mehrkar, A., Tomlinson, L., Douglas, I.J., Mathur, R., MacKenna, B., Ingelsby, P., Croker, R., Parry, J., Hester, F., Harper, S., DeVito, N.J., Hulme, W., Tazare, J., Smeeth, L., Goldacre, B., Eggo, R.M., 2021. Severity of SARS-CoV-2 alpha variant (B.1.1.7) in England. Clin. Infect. Dis. 6, ciab754.

Hall, V.J., Foulkes, S., Saei, A., Andrews, N., Oguti, B., Charlett, A., Wellington, E., Stowe, J., Gillson, N., Atti, A., Islam, J., Karagiannis, I., Munro, K., Khawam, J., Chand, M.A., Brown, C.S., Ramsay, M., Lopez-Bernal, J., Hopkins, S., Group, S.S., 2021. COVID-19 vaccine coverage in health-care workers in England and effectiveness of BNT162b2 mRNA vaccine against infection (SIREN): a prospective, multicentre, cohort study. Lancet 397, 1725–1735.

Han, P.C., Li, L.J., Liu, S., Wang, Q.S., Zhang, D., Xu, Z.P., Han, P., Li, X.M., Peng, Q., Su, C., Huang, B.H., Li, D.D., Zhang, R., Tian, M.X., Fu, L.T., Gao, Y.Z., Zhao, X., Liu, K.F., Qi, J.X., Gao, G.F., Wang, P.Y., 2022. Receptor binding and complex structures of human ACE2 to spike RBD from omicron and delta SARS-CoV-2. Cell 185, 630–640.

Harvey, W.T., Carabelli, A.M., Jackson, B., Gupta, R.K., Thomson, E.C., Harrison, E.M., Ludden, C., Reeve, R., Rambaut, A., Consortium, C.-G.U., Peacock, S.J., Robertson, D.L., 2021. SARS-CoV-2 variants, spike mutations and immune escape. Nat. Rev. Microbiol. 19, 409–424.

Hitchings, M.D.T., Ranzani, O.T., Dorion, M., D'Agostini, T.L., de Paula, R.C., de Paula, O.F.P., Villela, E.F.D., Torres, M.S.S., de Oliveira, S.B., Schulz, W., Almiron, M., Said, R., de Oliveira, R.D., Silva, P.V., de Araujo, W.N., Gorinchteyn, J.C., Andrews, J.R., Cummings, D.A.T., Ko, A.I., Croda, J., 2021. Effectiveness of ChAdOx1 vaccine in older adults during SARS-CoV-2 Gamma variant circulation in Sao Paulo. Nat. Commun. 12, 6220.

Katoh, K., Standley, D.M., 2013. MAFFT multiple sequence alignment software version 7: improvements in performance and usability. Mol. Biol. Evol. 30, 772–780.

Kraemer, M.U.G., Hill, V., Ruis, C., Dellicour, S., Bajaj, S., McCrone, J.T., Baele, G., Parag, K.V., Battle, A.L., Gutierrez, B., Jackson, B., Colquhoun, R., O'Toole, A., Klein, B., Vespignani, A., Volz, E., Faria, N.R., Aanensen, D.M., Loman, N.J., du Plessis, L., Cauchemez, S., Rambaut, A., Scarpino, S.V., Pybus, O.G., Consor, C.-G.U.C.-U., 2021. Spatiotemporal invasion dynamics of SARS-CoV-2 lineage B.1.1.7 emergence. Science 373, 889–895.

Kumar, S., Karuppanan, K., Subramaniam, G., 2022. Omicron (BA.1) and sub-variants (BA.1.1, BA.2, and BA.3) of SARS-CoV-2 spike infectivity and pathogenicity: a comparative sequence and structural-based computational assessment. J. Med. Virol. 94, 4780–4791.

Li, H., 2018. Minimap2: pairwise alignment for nucleotide sequences. Bioinformatics 34, 3094–3100.

Lin, S., Chen, Z.M., Zhang, X.D., Wen, A.O., Yuan, X., Yu, C.Z., Yang, J., He, B., Cao, Y., Lu, G.W., 2022. Characterization of SARS-CoV-2 Omicron spike RBD reveals significantly decreased stability, severe evasion of neutralizing-antibody recognition but unaffected engagement by decoy ACE2 modified for enhanced RBD binding. Signal Transduct. Targeted Ther. 7, 56.

Liu, C., Zhou, D., Nutalai, R., Duyvesteyn, H.M.E., Tuekprakhon, A., Ginn, H.M., Dejnirattisai, W., Supasa, P., Mentzer, A.J., Wang, B., Case, J.B., Zhao, Y., Skelly, D.T., Chen, R.E., Johnson, S.A., Ritter, T.G., Mason, C., Malik, T., Temperton, N., Paterson, N.G., Williams, M.A., Hall, D.R., Clare, D.K., Howe, A., Goulder, P.J.R., Fry, E.E., Diamond, M.S., Mongkolsapaya, J., Ren, J., Stuart, D.I., Screaton, G.R., 2022a. The antibody response to SARS-CoV-2 Beta underscores the antigenic distance to other variants. Cell Host Microbe 30, 53–68.

Liu, Y., Liu, J., Plante, K.S., Plante, J.A., Xie, X., Zhang, X., Ku, Z., An, Z., Scharton, D., Schindewolf, C., Widen, S.G., Menachery, V.D., Shi, P.Y., Weaver, S.C., 2022b. The

N501Y spike substitution enhances SARS-CoV-2 infection and transmission. Nature 602, 294–299.
Lubinski, B., Fernandes, M.H.V., Frazier, L., Tang, T., Daniel, S., Diel, D.G., Jaimes, J.A., Whittaker, G.R., 2022. Functional evaluation of the P681H mutation on the proteolytic activation of the SARS-CoV-2 variant B.1.1.7 (Alpha) spike. iScience 25, 103589.
Madhi, S.A., Baillie, V., Cutland, C.L., Voysey, M., Koen, A.L., Fairlie, L., Padayachee, S.D., Dheda, K., Barnabas, S.L., Bhorat, Q.E., Briner, C., Kwatra, G., Ahmed, K., Aley, P., Bhikha, S., Bhiman, J.N., Bhorat, A.E., du Plessis, J., Esmail, A., Groenewald, M., Horne, E., Hwa, S.H., Jose, A., Lambe, T., Laubscher, M., Malahleha, M., Masenya, M., Masilela, M., McKenzie, S., Molapo, K., Moultrie, A., Oelofse, S., Patel, F., Pillay, S., Rhead, S., Rodel, H., Rossouw, L., Taoushanis, C., Tegally, H., Thombrayil, A., van Eck, S., Wibmer, C.K., Durham, N.M., Kelly, E.J., Villafana, T.L., Gilbert, S., Pollard, A.J., de Oliveira, T., Moore, P.L., Sigal, A., Izu, A., Group, N.-S., Wits, V.C.G., 2021. Efficacy of the ChAdOx1 nCoV-19 Covid-19 vaccine against the B.1.351 variant. N. Engl. J. Med. 384, 1885–1898.
Moyo-Gwete, T., Madzivhandila, M., Mkhize, N.N., Kgagudi, P., Ayres, F., Lambson, B.E., Manamela, N.P., Richardson, S.I., Makhado, Z., van der Mescht, M.A., de Beer, Z., de Villiers, T.R., Burgers, W.A., Ntusi, N.A.B., Rossouw, T., Ueckermann, V., Boswell, M.T., Moore, P.L., 2022. Shared N417-dependent epitope on the SARS-CoV-2 omicron, beta, and delta plus variants. J. Virol. 96, e0055822.
Muik, A., Lui, B.G., Wallisch, A.K., Bacher, M., Muhl, J., Reinholz, J., Ozhelvaci, O., Beckmann, N., Garcia, R.D.G., Poran, A., Shpyro, S., Finlayson, A., Cai, H., Yang, Q., Swanson, K.A., Tureci, O., Sahin, U., 2022. Neutralization of SARS-CoV-2 Omicron by BNT162b2 mRNA vaccine-elicited human sera. Science 375, 678–680.
Nguyen, L.T., Schmidt, H.A., von Haeseler, A., Minh, B.Q., 2015. IQ-TREE: a fast and effective stochastic algorithm for estimating maximum-likelihood phylogenies. Mol. Biol. Evol. 32, 268–274.
Patone, M., Thomas, K., Hatch, R., San Tan, P., Coupland, C., Liao, W.Q., Mouncey, P., Harrison, D., Rowan, K., Horby, P., Watkinson, P., Hippisley-Cox, J., 2021. Mortality and critical care unit admission associated with the SARS-CoV-2 lineage B.1.1.7 in England: an observational cohort study. Lancet Infect. Dis. 21, 1518–1528.
Planas, D., Veyer, D., Baidaliuk, A., Staropoli, I., Guivel-Benhassine, F., Rajah, M.M., Planchais, C., Porrot, F., Robillard, N., Puech, J., Prot, M., Gallais, F., Gantner, P., Velay, A., Le Guen, J., Kassis-Chikhani, N., Edriss, D., Belec, L., Seve, A., Courtellemont, L., Pere, H., Hocqueloux, L., Fafi-Kremer, S., Prazuck, T., Mouquet, H., Bruel, T., Simon-Loriere, E., Rey, F.A., Schwartz, O., 2021. Reduced sensitivity of SARS-CoV-2 variant Delta to antibody neutralization. Nature 596, 276–280.
Radvak, P., Kwon, H.J., Kosikova, M., Ortega-Rodriguez, U., Xiang, R.X., Phue, J.N., Shen, R.F., Rozzelle, J., Kapoor, N., Rabara, T., Fairman, J., Xie, H., 2021. SARS-CoV-2 B.1.1.7 (alpha) and B.1.351 (beta) variants induce pathogenic patterns in K18-hACE2 transgenic mice distinct from early strains. Nat. Commun. 12, 6559.
Rajah, M.M., Hubert, M., Bishop, E., Saunders, N., Robinot, R., Grzelak, L., Planas, D., Dufloo, J., Gellenoncourt, S., Bongers, A., Zivaljic, M., Planchais, C., Guivel-Benhassine, F., Porrot, F., Mouquet, H., Chakrabarti, L.A., Buchrieser, J., Schwartz, O., 2021. SARS-CoV-2 Alpha, Beta, and Delta variants display enhanced Spike-mediated syncytia formation. EMBO J. 40, e108944.
Reed, L.J., Muench, H., 1938. A simple method of estimating fifty percent endpoints. Am. J. Hyg. 27, 493–497.
Sadoff, J., Gray, G., Vandebosch, A., Cardenas, V., Shukarev, G., Grinsztejn, B., Goepfert, P.A., Truyers, C., Fennema, H., Spiessens, B., Offergeld, K., Scheper, G., Taylor, K.L., Robb, M.L., Treanor, J., Barouch, D.H., Stoddard, J., Ryser, M.F., Marovich, M.A., Neuzil, K.M., Corey, L., Cauwenberghs, N., Tanner, T., Hardt, K., Ruiz-Guinazu, J., Le Gars, M., Schuitemaker, H., Van Hoof, J., Struyf, F., Douoguih, M., Group, E.S., 2021. Safety and efficacy of single-dose Ad26.COV2.S vaccine against Covid-19. N. Engl. J. Med. 384, 2187–2201.
Saito, A., Irie, T., Suzuki, R., Maemura, T., Nasser, H., Uriu, K., Kosugi, Y., Shirakawa, K., Sadamasu, K., Kimura, I., Ito, J., Wu, J.Q., Iwatsuki-Horimoto, K., Ito, M., Yamayoshi, S., Loeber, S., Tsuda, M., Wang, L., Ozono, S., Butlertanaka, E.P., Tanaka, Y.L., Shimizu, R., Shimizu, K., Yoshimatsu, K., Kawabata, R., Sakaguchi, T., Tokunaga, K., Yoshida, I., Asakura, H., Nagashima, M., Kazuma, Y., Nomura, R., Horisawa, Y., Yoshimura, K., Takaori-Kondo, A., Imai, M., Tanaka, S., Nakagawa, S., Ikeda, T., Fukuhara, T., Kawaoka, Y., Sato, K., G2P-Japan, G.P.J., 2022. Enhanced fusogenicity and pathogenicity of SARS-CoV-2 Delta P681R mutation. Nature 602, 300–306.
Sasaki, M., Uemura, K., Sato, A., Toba, S., Sanaki, T., 2021. SARS-CoV-2 variants with mutations at the S1/S2 cleavage site are generated in vitro during propagation in TMPRSS2-deficient cells. PLoS Pathog. 17, e1009233.
Sheikh, A., Robertson, C., Taylor, B., 2021. BNT162b2 and ChAdOx1 nCoV-19 vaccine effectiveness against death from the delta variant. N. Engl. J. Med. 385, 2195–2197.
Shinde, V., Bhikha, S., Hoosain, Z., Archary, M., Bhorat, Q., Fairlie, L., Lalloo, U., Masilela, M.S.L., Moodley, D., Hanley, S., Fouche, L., Louw, C., Tameris, M., Singh, N., Goga, A., Dheda, K., Grobbelaar, C., Kruger, G., Carrim-Ganey, N., Baillie, V., de Oliveira, T., Lombard Koen, A., Lombaard, J.J., Mngqibisa, R., Bhorat, A.E., Benade, G., Lalloo, N., Pitsi, A., Vollgraaff, P.L., Luabeya, A., Esmail, A., Petrick, F.G., Oommen-Jose, A., Foulkes, S., Ahmed, K., Thombrayil, A., Fries, L., Cloney-Clark, S., Zhu, M., Bennett, C., Albert, G., Faust, E., Plested, J.S., Robertson, A., Neal, S., Cho, I., Glenn, G.M., Dubovsky, F., Madhi, S.A., nCo, V.S.G., 2021. Efficacy of NVX-CoV2373 covid-19 vaccine against the B.1.351 variant. N. Engl. J. Med. 384, 1899–1909.
Shu, C.J., Huang, X., Tang, H.H., Mo, D.D., Zhou, J.W., Deng, C., 2021. Mutations in spike protein and allele variations in ACE2 impact targeted therapy strategies against SARS-CoV-2. Zool. Res. 42, 170–181.
Shuai, H., Chan, J.F., Hu, B., Chai, Y., Yuen, T.T., Yin, F., Huang, X., Yoon, C., Hu, J.C., Liu, H., Shi, J., Liu, Y., Zhu, T., Zhang, J., Hou, Y., Wang, Y., Lu, L., Cai, J.P., Zhang, A.J., Zhou, J., Yuan, S., Brindley, M.A., Zhang, B.Z., Huang, J.D., To, K.K., Yuen, K.Y., Chu, H., 2022. Attenuated replication and pathogenicity of SARS-CoV-2 B.1.1.529 Omicron. Nature 603, 693–699.
Singh, J., Rahman, S.A., Ehtesham, N.Z., Hira, S., Hasnain, S.E., 2021. SARS-CoV-2 variants of concern are emerging in India. Nat. Med. 27, 1131–1133.
Song, T.Z., Zheng, H.Y., Han, J.B., Jin, L., Yang, X., Liu, F.L., Luo, R.H., Tian, R.R., Cai, H.R., Feng, X.L., Liu, C., Li, M.H., Zheng, Y.T., 2020. Delayed severe cytokine storm and immune cell infiltration in SARS-CoV-2-infected aged Chinese rhesus macaques. Zool. Res. 41, 503–516.
Tang, P., Hasan, M.R., Chemaitelly, H., Yassine, H.M., Benslimane, F.M., Al Khatib, H.A., AlMukdad, S., Coyle, P., Ayoub, H.H., Al Kanaani, Z., Al Kuwari, E., Jeremijenko, A., Kaleeckal, A.H., Latif, A.N., Shaik, R.M., Rahim, H.F.A., Nasrallah, G.K., Al Kuwari, M.G., Al Romaihi, H.E., Butt, A.A., Al-Thani, M.H., Al Khal, A., Bertollini, R., Abu-Raddad, L.J., 2021. BNT162b2 and mRNA-1273 COVID-19 vaccine effectiveness against the SARS-CoV-2 Delta variant in Qatar. Nat. Med. 27, 2136–2143.
Tao, K., Tzou, P.L., Nouhin, J., Gupta, R.K., de Oliveira, T., Kosakovsky Pond, S.L., Fera, D., Shafer, R.W., 2021. The biological and clinical significance of emerging SARS-CoV-2 variants. Nat. Rev. Genet. 22, 757–773.
Tegally, H., Wilkinson, E., Giovanetti, M., Iranzadeh, A., Fonseca, V., Giandhari, J., Doolabh, D., Pillay, S., San, E.J., Msomi, N., Mlisana, K., von Gottberg, A., Walaza, S., Allam, M., Ismail, A., Mohale, T., Glass, A.J., Engelbrecht, S., Van Zyl, G., Preiser, W., Petruccione, F., Sigal, A., Hardie, D., Marais, G., Hsiao, N.Y., Korsman, S., Davies, M.A., Tyers, L., Mudau, I., York, D., Maslo, C., Goedhals, D., Abrahams, S., Laguda-Akingba, O., Alisoltani-Dehkordi, A., Godzik, A., Wibmer, C.K., Sewell, B.T., Lourenco, J., Alcantara, L.C.J., Kosakovsky Pond, S.L., Weaver, S., Martin, D., Lessells, R.J., Bhiman, J.N., Williamson, C., de Oliveira, T., 2021. Detection of a SARS-CoV-2 variant of concern in South Africa. Nature 592, 438–443.
van Loon, W., Rossig, H., Burock, S., Hofmann, J., Bernhard, J., Linzbach, E., Pettenkofer, D., Schonfeld, C., Gertler, M., Seybold, J., Kurth, T., Mockenhaupt, F.P., 2021. Emergence of SARS-CoV-2 B.1.1.7 lineage at outpatient testing site, Berlin, Germany , January March 2021. Emerg. Infect. Dis. 27, 1931–1934.
Wang, Y.D., Ma, Y.P., Xu, Y., Liu, J.Y., Li, X., Chen, Y.Y., Chen, Y., Xie, J., Xiao, L.B., Xiang, Z., Wu, F., Huang, J.H., 2022. Resistance of SARS-CoV-2 Omicron variant to convalescent and CoronaVac vaccine plasma. Emerg. Microb. Infect. 11, 424–427.
Xie, X.C., Han, J.B., Ma, G.Q., Feng, X.L., Li, X.H., Zou, Q.C., Deng, Z.H., Zeng, J.X., 2021. Emerging SARS-CoV-2 B.1.621/Mu variant is prominently resistant to inactivated vaccine-elicited antibodies. Zool. Res. 42, 789–791.
Xu, L., Yu, D.D., Ma, Y.H., Yao, Y.L., Luo, R.H., Feng, X.L., Cai, H.R., Han, J.B., Wang, X.H., Li, M.H., Ke, C.W., Zheng, Y.T., Yao, Y.G., 2020. COVID-19-like symptoms observed in Chinese tree shrews infected with SARS-CoV-2. Zool. Res. 41, 517–526.
Zeng, J., Dong, S., Luo, Z., Xie, X., Fu, B., Li, P., Liu, C., Yang, X., Chen, Y., Wang, X., Liu, Z., Wu, J., Yan, Y., Wang, F., Chen, J.F., Zhang, J., Long, G., Goldman, S.A., Li, S., Zhao, Z., Liang, Q., 2020. The zika virus capsid disrupts corticogenesis by suppressing Dicer activity and miRNA biogenesis. Cell Stem Cell 27, 618–632.e9.
Zeng, J., Wang, Y., Luo, Z., Chang, L.C., Yoo, J.S., Yan, H., Choi, Y., Xie, X., Deverman, B.E., Gradinaru, V., Gupton, S.L., Zlokovic, B.V., Zhao, Z., Jung, J.U., 2019. TRIM9-mediated resolution of neuroinflammation confers neuroprotection upon ischemic stroke in mice. Cell Rep. 27, 549–560 e6.
Zeng, J., Xie, X., Feng, X.L., Xu, L., Han, J.B., Yu, D., Zou, Q.C., Liu, Q., Li, X., Ma, G., Li, M.H., Yao, Y.G., 2022. Specific inhibition of the NLRP3 inflammasome suppresses immune overactivation and alleviates COVID-19 like pathology in mice. EBioMedicine 75, 103803.
Zhang, H., Deng, S.S., Ren, L.T., Zheng, P.Y., Hu, X.W., Jin, T.C., Tan, X., 2021. Profiling CD8(+) T cell epitopes of COVID-19 convalescents reveals reduced cellular immune responses to SARS-CoV-2 variants. Cell Rep. 36, 109708.
Zhang, L.Z., Jackson, C.B., Mou, H.H., Ojha, A., Peng, H.Y., Quinlan, B.D., Rangarajan, E.S., Pan, A.D., Vanderheiden, A., Suthar, M.S., Li, W.H., Izard, T., Rader, C., Farzan, M., Choe, H., 2020. SARS-CoV-2 spike-protein D614G mutation increases virion spike density and infectivity. Nat. Commun. 11, 6013.
Zhao, H.J., Lu, L., Peng, Z., Chen, L.L., Meng, X.J., Zhang, C.Y., Ip, J.D., Chan, W.M., Chu, A.W.H., Chan, W.H., Jin, D.Y., Chen, H.L., Yuen, W.Y., To, K.K.W., 2022. SARS-CoV-2 Omicron variant shows less efficient replication and fusion activity when compared with Delta variant in TMPRSS2-expressed cells. Emerg. Microb. Infect. 11, 277–283.

Virologica Sinica

Supplementary Data

Characteristics of replication and pathogenicity of SARS-CoV-2 Alpha and Delta isolates

Xiao-Li Feng [a,1], Dandan Yu [a,b,f,1], Mi Zhang [c,1], Xiaohong Li [b,1], Qing-Cui Zou [a], Wentai Ma [d], Jian-Bao Han [a], Ling Xu [a,b,f], Cuixian Yang [c], Wang Qu [a], Zhong-Hua Deng [a], Junyi Long [a], Yanghaopeng Long [a], Mingkun Li [d,e], Yong-Gang Yao [a,b,f,g], Xing-Qi Dong [c,*], Jianxiong Zeng [a,b,f,g,h,*], Ming-Hua Li [a,*]

[a] *Kunming National High-level Biosafety Research Center for Non-Human Primates, Center for Biosafety Mega-Science, Kunming Institute of Zoology, Chinese Academy of Sciences, Kunming, 650107, China*
[b] *Key Laboratory of Animal Models and Human Disease Mechanisms of the Chinese Academy of Sciences, and KIZ-CUHK Joint Laboratory of Bioresources and Molecular Research in Common Diseases, Kunming Institute of Zoology, Chinese Academy of Sciences, Kunming, 650201, China*
[c] *Department of Infectious Diseases, Yunnan Provincial Infectious Diseases Hospital, Kunming, 650301, China*
[d] *Key Laboratory of Genomic and Precision Medicine, Beijing Institute of Genomics, Chinese Academy of Sciences, and China National Center for Bioinformation, Beijing, 100101, China.*
[e] *Center for Excellence in Animal Evolution and Genetics, Chinese Academy of Sciences, Kunming, 650201, China*
[f] *National Resource Center for Non-Human Primates, National Research Facility for Phenotypic & Genetic Analysis of Model Animals (Primate Facility), Kunming Institute of Zoology, Chinese Academy of Sciences, Kunming, 650107, China*
[g] *Kunming College of Life Science, University of Chinese Academy of Sciences, Kunming, 650204, China*
[h] *Yunnan Key Laboratory of Biodiversity Information, Kunming Institute of Zoology, Chinese Academy of Sciences, Kunming, 650201, China*

[*] Corresponding authors.
E-mail addresses: dongxq8001@126.com (X.Q. Dong), zengjianxiong@mail.kiz.ac.cn (J. Zeng), limh@mail.kiz.ac.cn (M.H. Li)

[1] Xiao-Li Feng, Dandan Yu, Mi Zhang and Xiaohong Li contributed equally to this work.

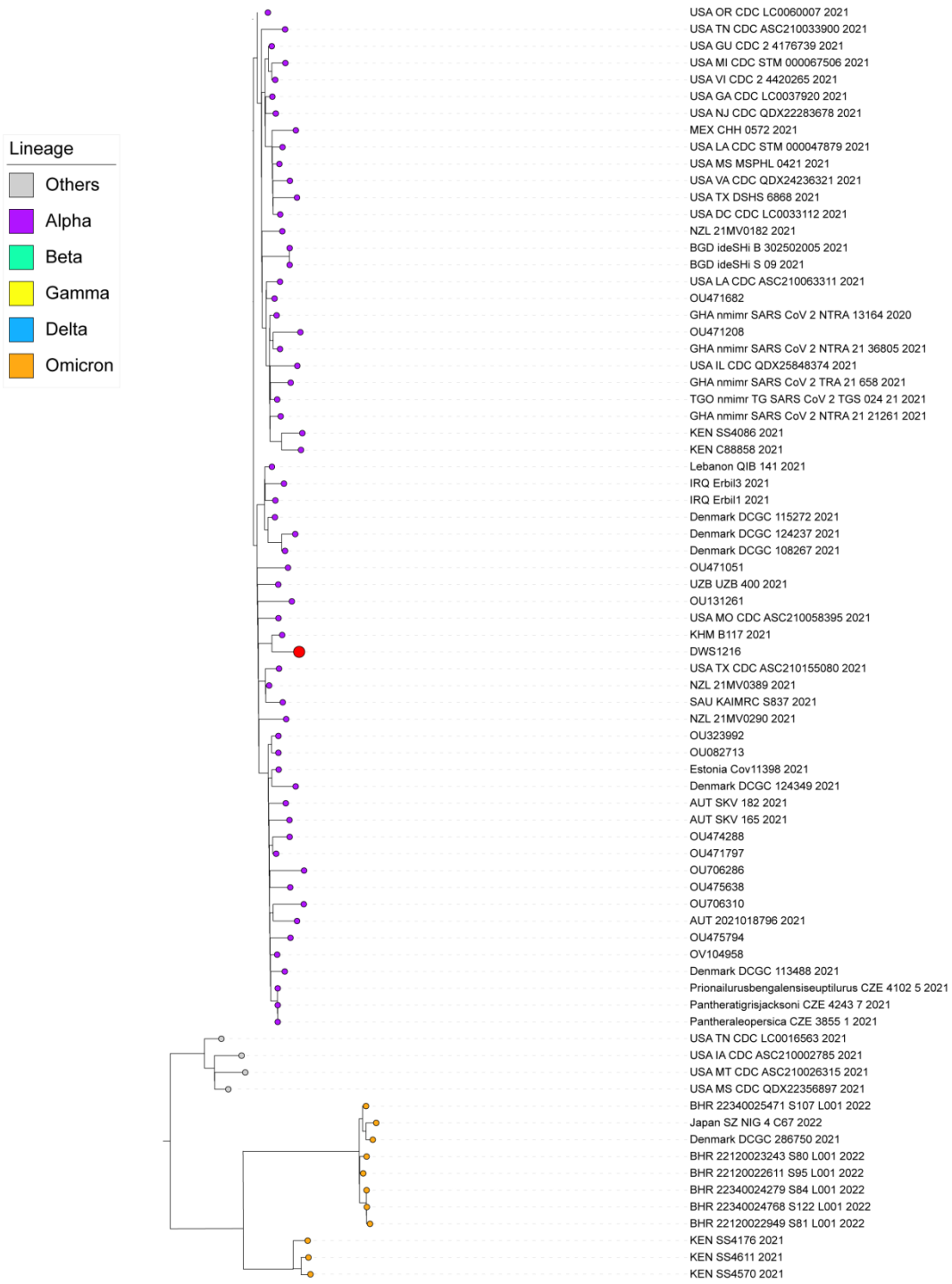

Supplementary Fig. S1 Phylogenetic tree of the Alpha isolate. Phylogenetic analysis of the Spike sequences of the Alpha isolate (red circle) within the existed SARS-CoV-2 Alpha variants (purple circle) by Nextstrain (Dated on 8 Feb 2022).

Supplementary Fig. S2 Phylogenetic tree of the Delta isolate. Phylogenetic analysis of the Spike sequences of the Delta isolate (red circle) within the existed SARS-CoV-2 Delta variants (blue circle) by Nextstrain (Dated on 8 Feb 2022).

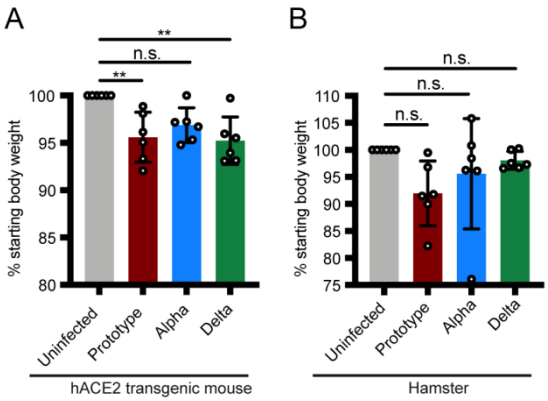

Supplementary Fig. S3 Body weight of infected hACE2 transgenic mice and hamsters. **A, B** Body weight was monitored at 3 dpi and indicated by percentage of starting body weight for the prototype SARS-CoV-2-, Alpha- and Delta-infected hACE2 transgenic mice (**A**) and hamsters (**B**). The uninfected animals were used as control. Data were shown as mean ± standard deviaion (n = 6). Statistical analysis was performed by one-way ANOVA with Bonferroni's *post hoc* test. n.s., not significant, $^{**}P < 0.01$.

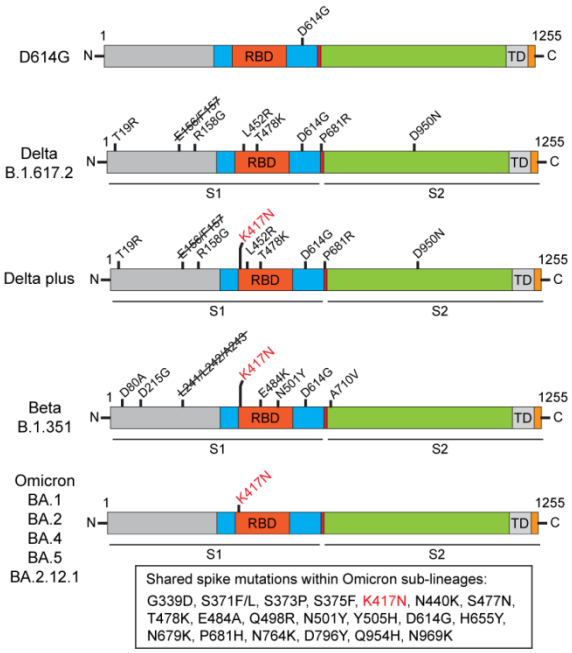

Supplementary Fig. S4 Spike K417N mutation in SARS-CoV-2 variants. Diagram of spike mutations including K417N of indicated SARS-CoV-2 variants.

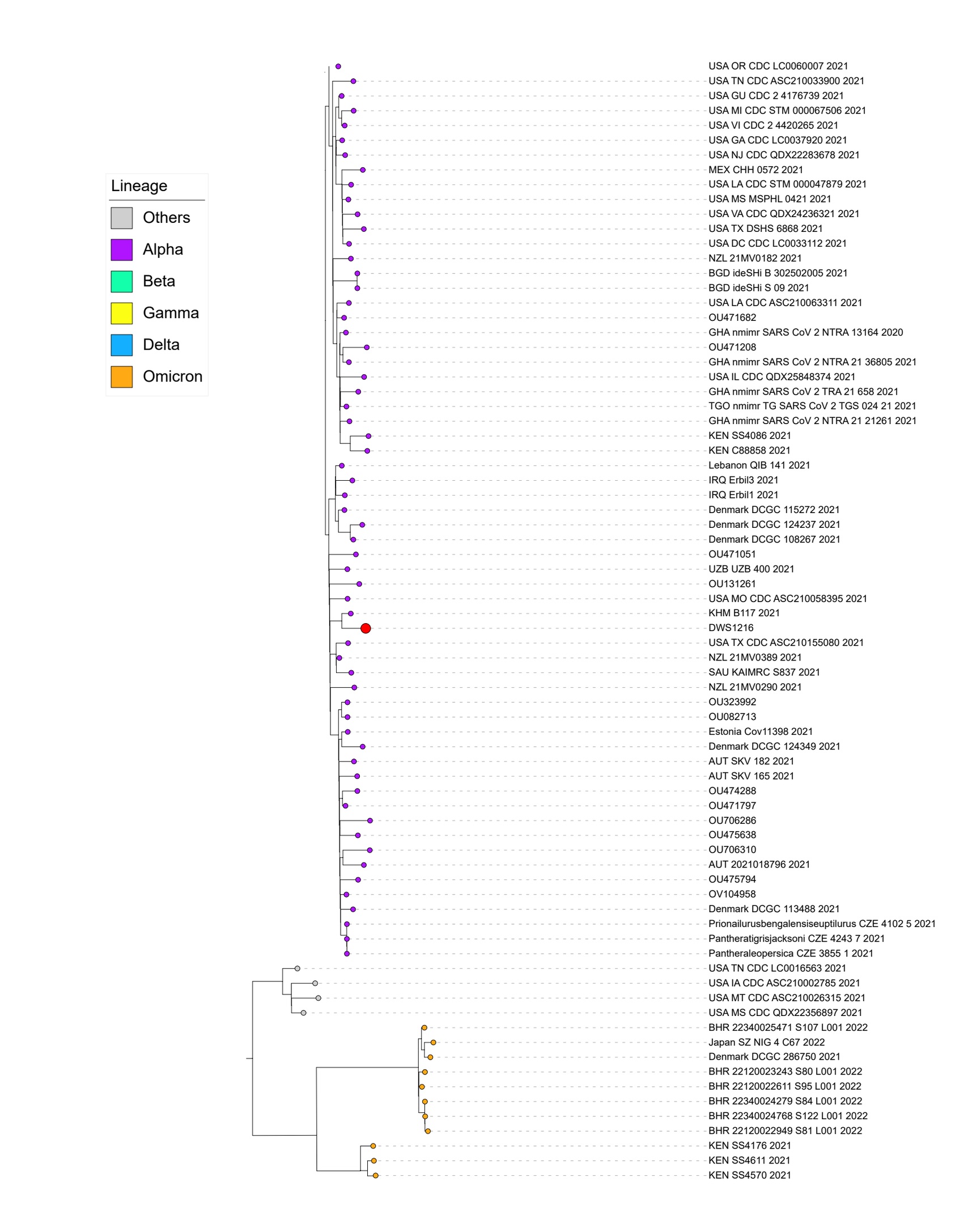
Lineage
Others
Alpha
Beta
Gamma
Delta
Omicron
USA OR CDC LC0060007 2021
USA TN CDC ASC210033900 2021
USA GU CDC 2 4176739 2021
USA MI CDC STM 000067506 2021
USA VI CDC 2 4420265 2021
USA GA CDC LC0037920 2021
USA NJ CDC QDX22283678 2021
MEX CHH 0572 2021
USA LA CDC STM 000047879 2021
USA MS MSPHL 0421 2021
USA VA CDC QDX24236321 2021
USA TX DSHS 6868 2021
USA DC CDC LC0033112 2021
NZL 21MV0182 2021
BGD ideSHi B 302502005 2021
BGD ideSHi S 09 2021
USA LA CDC ASC210063311 2021
OU471682
GHA nmimr SARS CoV 2 NTRA 13164 2020
OU471208
GHA nmimr SARS CoV 2 NTRA 21 36805 2021
USA IL CDC QDX25848374 2021
GHA nmimr SARS CoV 2 TRA 21 658 2021
TGO nmimr TG SARS CoV 2 TGS 024 21 2021
GHA nmimr SARS CoV 2 NTRA 21 21261 2021
KEN SS4086 2021
KEN C88858 2021
Lebanon QIB 141 2021
IRQ Erbil3 2021
IRQ Erbil1 2021
Denmark DCGC 115272 2021
Denmark DCGC 124237 2021
Denmark DCGC 108267 2021
OU471051
UZB UZB 400 2021
OU131261
USA MO CDC ASC210058395 2021
KHM B117 2021
DWS1216
USA TX CDC ASC210155080 2021
NZL 21MV0389 2021
SAU KAIMRC S837 2021
NZL 21MV0290 2021
OU323992
OU082713
Estonia Cov11398 2021
Denmark DCGC 124349 2021
AUT SKV 182 2021
AUT SKV 165 2021
OU474288
OU471797
OU706286
OU475638
OU706310
AUT 2021018796 2021
OU475794
OV104958
Denmark DCGC 113488 2021
Prionailurusbengalensiseuptilurus CZE 4102 5 2021
Pantheratigrisjacksoni CZE 4243 7 2021
Pantheraleopersica CZE 3855 1 2021
USA TN CDC LC0016563 2021
USA IA CDC ASC210002785 2021
USA MT CDC ASC210026315 2021
USA MS CDC QDX22356897 2021
BHR 22340025471 S107 L001 2022
Japan SZ NIG 4 C67 2022
Denmark DCGC 286750 2021
BHR 22120023243 S80 L001 2022
BHR 22120022611 S95 L001 2022
BHR 22340024279 S84 L001 2022
BHR 22340024768 S122 L001 2022
BHR 22120022949 S81 L001 2022
KEN SS4176 2021
KEN SS4611 2021
KEN SS4570 2021

Switzerland BE IFIK 3867 2740 2021
OV113328
Scotland QEUH 17E2EB5 2021
England BRBR 2C703A6 2021
OV224999
England MILK 2D26089 2021
England BRBR 283A5F1 2021
England MILK 27414A0 2021
OV522270
England LSPA 2C2D214 2021
Scotland QEUH 2780126 2021
OV662786
OV511540
OV531480
OV360844
OV109542
OV661767
England QEUH 2EBE085 2021
England PLYM 2CD09B1 2021
Denmark DCGC 286751 2021
England MILK 2D395B1 2021
Scotland QEUH 29A0CA5 2021
Scotland QEUH 2770772 2021
KEN SS4387 2021
KEN SS4165 2021
England ALDP 29E44DA 2021
Scotland QEUH 2D1AF6D 2021
England MILK 2CD9D34 2021
England MILK 2BF638B 2021
DWSJ070
USA GA GPHL 2509 2021
USA UT CDC ASC210489950 2021
KEN SS3858 2021
JAM 202112090 2021
JAM 202112039 2021
JAM 202112041 2021
JAM 202112033 2021
USA SRL 330921312 2021
JAM 202112079 2021
JAM 202112014 2021
Liechtenstein FL Risch 21A0405459 2021
Japan SZ NIG Y212189 2021
Japan SZ NIG 3 C13000 2021
Japan SZ NIG 3 C12825 2021
Japan SZ NIG Y212197 2021
Japan SZ NIG Y212196 2021
Japan SZ NIG Y212211 2021
Japan SZ NIG 215866 2021
Japan SZ NIG Y212208 2021
Japan SZ NIG 215861 2021
Japan SZ NIG Y212209 2021
Japan SZ NIG Y212251 2022
Japan SZ NIG Y212250 2022
Japan SZ NIG 3 C13089 2021
Japan SZ NIG 3 C13090 2021
Japan SZ NIG 3 C13091 2021
Japan SZ NIG 3 C13086 2021
Japan SZ NIG Y212184 2021
Japan SZ NIG 3 C12214 2021
Japan SZ NIG Y211900 2021
Japan SZ NIG 4 C82 2022
Japan SZ NIG 4 C197 2022
Japan SZ NIG Y212248 2022
Japan SZ NIG Y212247 2022
OV377479
OV282707
USA DC CDC LC0343827 2021
Liechtenstein FL Risch 21C0317059 2021
Liechtenstein FL Risch 21C1613065 2021
Liechtenstein FL Risch 21B0918297 2021
England QEUH 2C0722F 2021
USA OH CDC ASC210631536 2021
England LSPA 2FF050F 2021
England ALDP 2A4D6C9 2021
USA IN CDC LC0322798 2021
USA VI CDC STM 000739061 2021

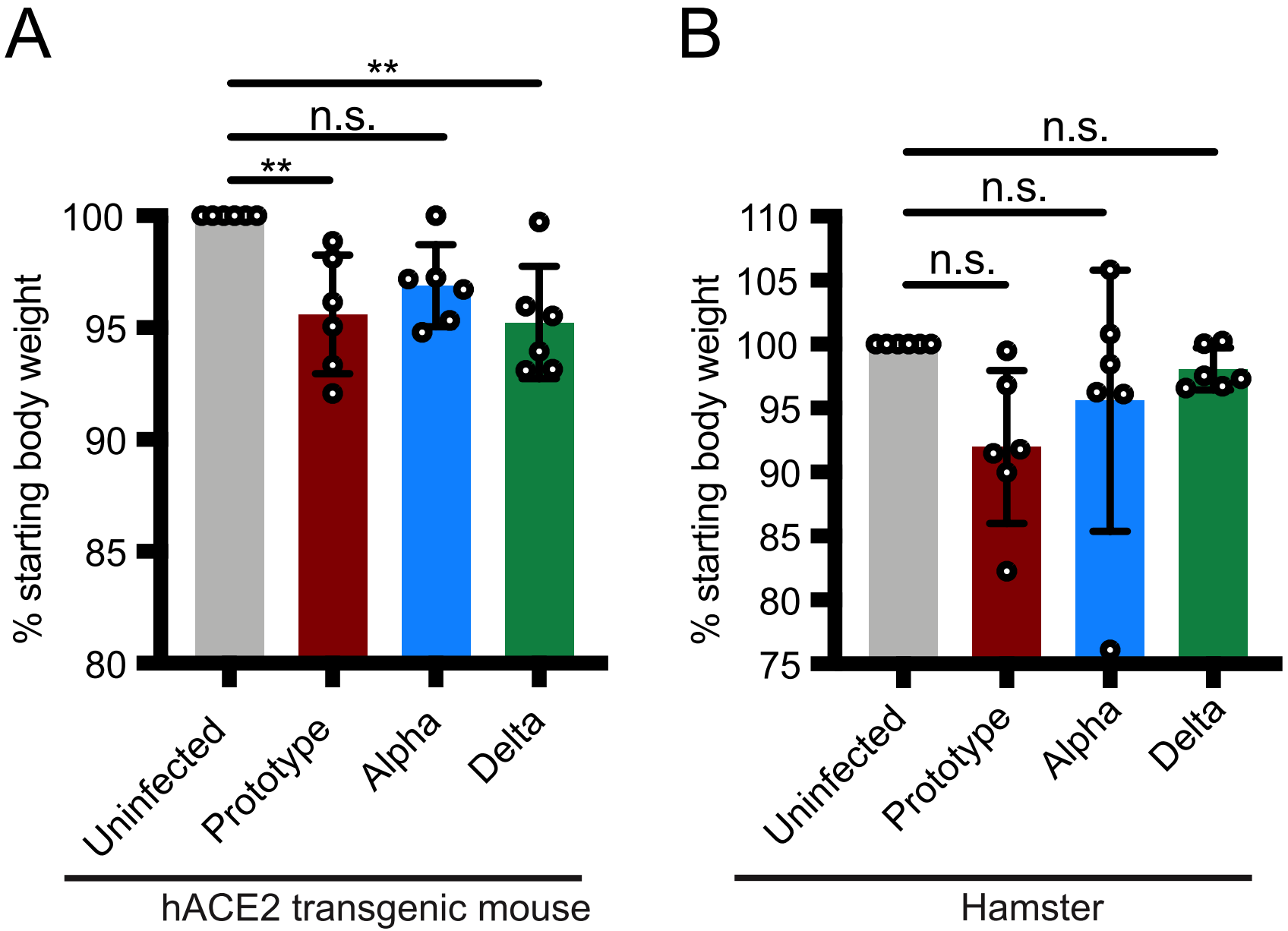
A
**
n.s.
**
100
95
90
85
80
% starting body weight
Uninfected
Prototype
Alpha
Delta
hACE2 transgenic mouse
B
n.s.
n.s.
n.s.
110
105
100
95
90
85
80
75
% starting body weight
Uninfected
Prototype
Alpha
Delta
Hamster

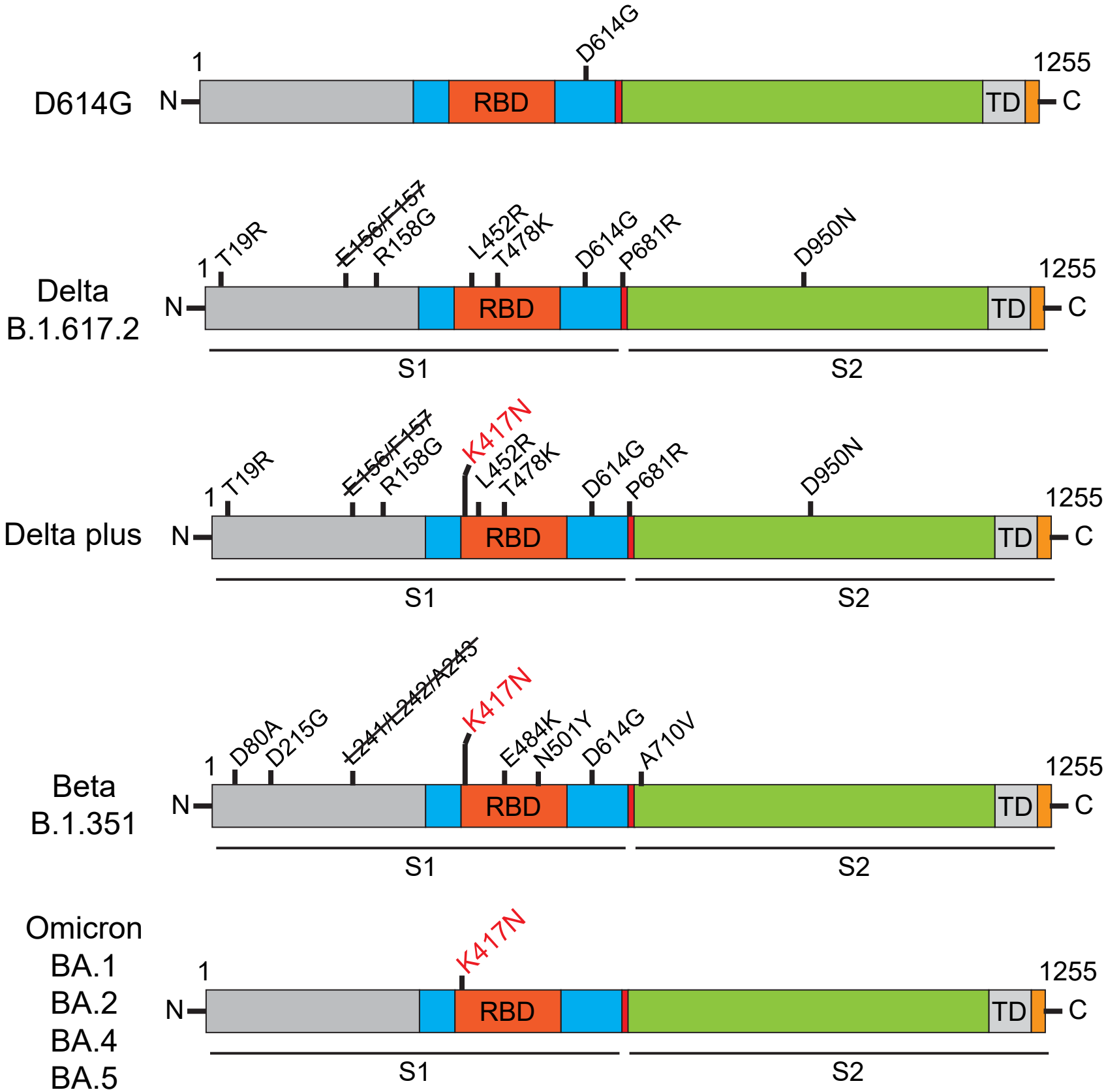

Shared spike mutations within Omicron sub-lineages:

G339D, S371F/L, S373P, S375F, K417N, N440K, S477N, T478K, E484A, Q498R, N501Y, Y505H, D614G, H655Y, N679K, P681H, N764K, D796Y, Q954H, N969K